



ERNEST ORLANDO LAWRENCE BERKELEY NATIONAL LABORATORY

X-Ray Based Sub-Picosecond Electron Bunch Characterization Using 90° Thomson Scattering

W. Leemans, R.W. Schoenlein, P. Volfbeyn,
A. Chin, T.E. Glover, P. Balling, M. Zolotarev,
K.J. Kim, S. Chattopadhyay, and C.V. Shank
**Accelerator and Fusion
Research Division**

June 1996
Submitted to
Physical Review Letters

LOAN COPY
Circulates
for 4 weeks

Bldg. 50 Library.
Copy 2

LBNL-39060

X-ray based sub-picosecond electron bunch characterization using 90° Thomson scattering*

W. Leemans^a, R.W. Schoenlein^b, P. Volfbeyn^a, A. Chin^c, T.E. Glover^b, P. Balling^b,
M. Zolotarev^a, K.J. Kim^a, S. Chattopadhyay^a, and C.V. Shank^{b, c}
Center for Beam Physics
Lawrence Berkeley National Laboratory
University of California
Berkeley, California 94720

June 1996

^a Accelerator and Fusion Research Division-Center for Beam Physics

^b Materials Sciences Division, Ernest Orlando Lawrence Berkeley National Laboratory

^c Physics Department, University of California at Berkeley

* This work was supported by the Director, Office of Energy Research, Office of Basic Energy Sciences, US Department of Energy, Under Contract No. DE-AC03-76SF00098 and FDDEFG-03-95ER-40936 and by the National Science Foundation under Grant No. PHY-9512693.

X-ray based sub-picosecond electron bunch characterization using 90° Thomson scattering

W. P. Leemans^a, R. W. Schoenlein^b, P. Volfbeyn^a, A. Chin^c, T. E. Glover^b, P. Balling^b,
M. Zolotarev^a, K.J. Kim^a, S. Chattopadhyay^a, and C.V. Shank^{b,c}

^aAccelerator and Fusion Research Division-Center for Beam Physics

^bMaterial Sciences Division

Ernest Orlando Lawrence Berkeley National Laboratory

^cPhysics Department

University of California at Berkeley

Abstract

X-rays produced by Thomson scattering of a short terawatt laser pulse (40 mJ, 100fs long) off a 50 MeV electron beam at 90°, are shown to be an effective diagnostic to measure transverse and longitudinal density distributions of the electron beam with subpicosecond time resolution. Near infrared (800 nm) laser pulses, were focused onto the electron beam waist, generating x-rays in the forward direction with energies up to 30 keV. The transverse and longitudinal electron beam dimensions have been obtained by measuring the intensity of the x-ray beam, while scanning the laser beam across the electron beam in space and time. The electron beam divergence has been obtained through measurement of spatial and spectral characteristics of the scattered x-ray beam.

PACS.:13.60.Fz, 29.27.Fh, 29.30.Kv.

The advent of sub-picosecond terawatt laser systems based on chirped pulse amplification [1], has renewed the interest in bright sources of high-energy photons that employ scattering between laser light and relativistic electrons [2,3], as well as in diagnostics and control of relativistic particle beams [4]. Production of femtosecond x-ray pulses using such scattering requires either development of very short electron bunches [5] or a scattering geometry in which the photon and electron beams cross at 90° and are both tightly focused [3]. In this geometry the interaction time between the electron beam and laser beam is limited to the transverse rather than the longitudinal transit time of the laser pulse across the electron beam. Ultra-short x-ray pulses can then be generated from long electron bunches [6]. In this Letter we will present results demonstrating another fascinating and immediate consequence of the 90° scattering geometry. Namely, the possibility to measure the phase space properties of femtosecond length electron beam slices.

Historically, soon after the invention of the laser, Fiocco and Thompson [7] used Thomson scattering to measure the energy distribution of an electron beam. Recently, transverse e-beam sizes as small as 70 nm were measured by scanning a high energy electron beam across the intensity fringes of an optical standing wave [8]. With femtosecond laser pulses, longitudinally resolved measurement of e-beam phase space characteristics becomes possible. Development of this kind of techniques will be increasingly important for diagnosing electron bunches in future accelerators.

Figure 1 presents a schematic of the experiment in which the 90° Thomson scattering geometry has been used. The experiments are conducted at the Beam Test Facility (BTF) [9] of the Center for Beam Physics at the Berkeley Laboratory. The linear accelerator (linac) injector of the Advanced Light Source is used in conjunction with a terawatt short pulse laser system. Electron bunches with energy of 50 MeV (energy spread 0.2 - 0.4 %) containing typically 1.3 nC of charge within a 10-15 ps (rms) bunch length, are produced by the linac at a 2 Hz repetition rate, and transported using bend

magnets and quadrupoles (BTF line) to an interaction chamber. The electron beam is focused in the interaction chamber where it scatters against the laser beam. After the interaction chamber, a 60° bend magnet deflects the electron beam onto a beam dump, away from the forward scattered x-rays.

To measure the spot size (and position) of the electron beam at the interaction point (IP), a 2 μm thick Al-coated nitrocellulose foil, mounted on a retractable plunger at 45° with respect to the beam, was installed in the chamber. An image of the electron beam was obtained from optical transition radiation (OTR) [10], which is produced when an electron beam crosses a foil. The image was relayed onto a 16 bit CCD camera or optical streak camera using a small f-number telescope. The spatial resolution of the imaging system was 14 μm . Electron spot sizes as small as 35 μm have been measured.

The femtosecond laser system is based on chirped pulse amplification in Ti:Al₂O₃ [1, 11]. The Kerr lens modelocked oscillator operates at the fourth sub-harmonic of the 500 MHz master oscillator source for the linac. Individual laser oscillator pulses are extracted at a 10 Hz repetition rate, and are stretched using a grating and a telescope based on a parabolic reflector. Amplification to the 100 - 200 mJ range is achieved in an 8-pass pre-amplifier and a 3-pass power amplifier pumped by a Q-switched Nd:YAG laser. The amplified pulses are compressed in a vacuum chamber using a grating pair and are propagated to the e-beam/laser interaction chamber through an evacuated beam line. Amplified laser pulses as short as 50 fs (2 TW peak power) have been produced but typical operating parameters for the experiment are 100 fs long pulses containing about 40 mJ energy. A 75 cm radius of curvature mirror is used to focus the S-polarized amplified laser pulses to about a 30 μm diameter spot at the IP (measured by a CCD camera at an equivalent image plane outside the vacuum chamber).

Synchronization between the laser oscillator and linac is accomplished by using a phase-locked loop which dynamically adjusts the oscillator cavity length. The phase

error signal is generated by mixing the fourth harmonic of the oscillator repetition frequency (generated from a photo-diode) with the master oscillator source for the linac. Timing jitter measurements (using a streak camera with time resolution of 1.5 - 2 ps) which simultaneously detects a laser pulse and OTR from the electron bunch indicate an rms jitter of 1-2 ps.

To monitor the arrival time of the electron bunch and laser pulse at the IP, a button-type radio-frequency pick-up, and a 6 ps rise time photoconductive switch, were used to provide a signal from the electron beam and laser pulse, respectively. The signals were measured on a transient digitizer with 4.5 GHz bandwidth. An optical delay line was used to change the arrival time of the laser pulse. Initial spatial alignment of the beams was accomplished by optimizing the e-beam and laser transmission through a cube with two 250 μm diameter intersecting orthogonal holes.

Total flux and profile of the x-ray beam, were measured using a phosphor screen[12], located 80 cm from the IP. This phosphor has a linear energy conversion efficiency in the 10 - 50 keV range [13]. Visible photons from the screen are imaged onto a 16 bit CCD camera [14]. The sensitivity of the x-ray detection system was calibrated using a NIST traceable I^{129} radioactive source. For a horizontal and vertical CCD binning factor of 32, the sensitivity (x-rays/CCD count) of the system was measured to be 1.2 ± 0.4 x-ray photons/count, and was found to be linear over at least two orders of magnitude. The detection system had a full collection angle of 25 mrad. The total flux within the collection angle was typically 5×10^4 photons.

To measure the transverse electron beam distribution for a given slice of the electron beam, we scanned the laser beam transversely across the electron beam and monitored the x-ray yield on the phosphor screen. The laser beam was moved by changing the vertical tilt of the focusing mirror in steps of 10 μm and the plot of x-ray yield vs. laser position is shown in Fig.(2). From the data we find a vertical rms spot size

of 56 μm . This result is in good agreement with an independent measurement of the transverse e-beam size using the OTR image on the CCD camera (Fig.2), which gives 40 μm and 57 μm in the horizontal and vertical direction respectively.

Measurement of the electron beam divergence for a fixed longitudinal location (i.e. fixed delay time between the laser and electron beam), was done by monitoring the spatial x-ray beam profile on the phosphor screen. A typical x-ray image on the phosphor screen from a femtosecond electron beam slice is shown in Fig. 3a, and horizontal and vertical line-outs are shown in Fig.3b. Background radiation from electron Bremsstrahlung has been subtracted.

To analyze the experimentally measured spatial and spectral characteristics of the x-ray beam, we have convolved the single electron Thomson scattering cross-section with a Gaussian spatial and spectral distribution of photons and electrons. For our parameters, any non-linear dependence of the quiver motion on the field of the laser can be neglected as well as any recoil effects of the electron (hence Thomson as opposed to Compton scattering). The energy of the scattered x-ray photon U_x , for an incident single photon with frequency ω_0 , is given by (for $\gamma \gg 1$) [2, 3]

$$U_x = \frac{2\gamma^2 \hbar \omega_0}{1 + \gamma^2 \chi^2} (1 - \cos \psi) \quad (1).$$

Here ψ is the interaction angle between the electron and laser beam ($\psi = \pi/2$ in our experiments), and $\chi \ll 1$ is the scattering angle.

The scattered x-ray energy flux can be obtained by accounting for the spatial and temporal profiles of the electron and laser beams as well as by convolving the single electron spectrum [3], with the angular distribution function of the electron beam, and integrating over all energies and azimuthal angles.

For a Gaussian angular electron beam distribution and a linear polarized incident laser beam, in x-direction (see Fig. 1), we obtain, at the horizontal (vertical) observation angles θ_x (θ_y)

$$\frac{dP}{d\theta_x d\theta_y} \propto \int_0^{2\pi} d\phi \int_0^1 d\kappa F(\kappa) \kappa [1 - 4\kappa(1 - \kappa) \cos^2 \phi] \exp\left[-\frac{(\theta_x - \gamma^{-1} \sqrt{\frac{1}{\kappa} - 1} \cos \phi)^2}{2\sigma_{\theta_x}^2}\right] \exp\left[-\frac{(\theta_y + \gamma^{-1} \sqrt{\frac{1}{\kappa} - 1} \sin \phi)^2}{2\sigma_{\theta_y}^2}\right] \quad (2).$$

Here σ_{θ_x} and σ_{θ_y} are the rms widths of the angular distribution of the electron beam in the horizontal and vertical direction respectively, and $F(\kappa)$ is an x-ray energy dependent function which takes into account overall detector sensitivity. We also defined $\kappa = U/U_{\max} = (1 + \gamma^2 \chi^2)^{-1}$ from Eqn.(1), where $U_{\max} = 2\gamma^2 \hbar \omega_0$ and assumed a single incident laser frequency.

By fitting the line-out data (see Fig. 3b) using Eqn.(2), we obtain an electron beam divergence of σ_{θ_x} (σ_{θ_y}) = 6.3 ± 0.2 (3.9 ± 0.2) mrad. The difference between σ_{θ_x} and σ_{θ_y} , is due to a combination of, the electron beam being focused astigmatically at the IP, resulting in a tilted phase space ellipse (y, y'), and a laser spot size much smaller than the vertical electron beam size. As the laser beam crosses the focal volume of the electron beam, the complete horizontal (direction of propagation of the laser) phase space (x, x') is sampled by the laser beam. However, only electrons occupying the region in the vertical phase space defined by the spatial overlap with the laser beam will contribute to the x-ray flux. As opposed to the transition radiation based detector, the laser beam therefore acts as an optical microprobe of a finite region of the transverse phase space.

To have an independent estimate of the electron beam divergence, we analyzed X-ray spectra measured at angles $\theta = 0, 5, \text{ and } 10$ mrad [6], and used the fact that for a

fixed observation angle θ , the shape of the x-ray spectrum is dependent on the beam parameters. For an electron beam focused to a spot size of 70 μm at the IP, these spectra indicated an effective angular divergence of the electron beam of 3.5 - 4 mrad.

The spot size measurements and beam divergence measurements imply a horizontal geometric slice emittance $\sigma_x \sigma_{\theta x}$ for the electron beam of 0.25 ± 0.03 mm-mrad. A linac beam emittance of 0.32 ± 0.02 mm-mrad, was previously measured using a time-integrated quadrupole scan technique [15], which is in reasonable agreement with the x-ray slice measurements.

To measure the longitudinal electron beam distribution, the x-ray flux on the phosphor screen was monitored as a function of the delay between laser and e-beam (changed in 1 ps time steps). These data (Fig.4a), are a direct measure of the longitudinal electron beam distribution at the IP, and typically showed a 5 ps wide peak sitting on a 20 ps wide pedestal. The amplitude of the narrow peak was typically 2-3 times larger than the pedestal. The detail seen in the longitudinal distribution is in contrast to the time resolved OTR from the streak camera which typically showed a 25-30 ps wide electron beam without any sharp time structure (Fig. 4b). Analyzing the different causes for this observation, we recognized that the measurements can be very sensitive to small correlated energy spread of the electron bunch. For an electron bunch which exhibits a finite time-correlated energy spread (chirp), each time slice will reach focus at a different longitudinal location due to finite chromaticity in the focusing optics. Magnetic lattice calculations with MAD [16] indicate that, for an energy chirp of 0.25 %, the vertical spot size increases by a factor two, compared to best focus. This change in vertical overlap between the laser and electron beam, may be large enough to explain the observations but a more complete study is necessary.

In summary, we have presented first experimental results of an electron beam diagnostic based on x-ray measurements from 90° Thomson scattering of femtosecond

laser light. The total flux of x-rays was on the order of 5×10^4 for typical laser and electron beam parameters in the experiment. From a study of x-ray beam images and total flux, we have obtained the transverse electron beam phase space distribution of essentially a 300 fs slice of the electron beam. By scanning the laser beam in time along the electron bunch, we have measured not only the longitudinal density distribution, but also found that the Thomson scattering technique can become a powerful tool to measure longitudinal phase space properties. Electron beam diagnostics with capability of measuring phase space properties with femtosecond time resolution will become increasingly important for understanding of electron bunch dynamics in future accelerators.

One of us (WPL) would like to thank E. Esarey for useful conversations. We also would like to thank L. Archambault, A. Belkacem, T. Byrne, M. Conde, M. de Loos, J. Dougherty, M. Faiguenblatt, A. Ghiorso, H. Gould, R. Govil, A. Jackson, D. Massoletti, B. van der Geer and A. Zholents for their contributions.

This work is supported by the Department of Energy under Contract No. AC03-76SF00098 and FDDEFG-03-95ER-40936 and by the National Science Foundation under Grant No. PHY-9512693. One of us (P.B.) gratefully acknowledges the support of the Danish Natural Science Research Council (SNF).

References

- [1] D. Strickland and G. Mourou, *Opt. Comm.* **56**, 219 (1985).
- [2] P. Sprangle, et al., *J. Appl. Phys.* **72**, 5032 (1992).
- [3] K.J. Kim, S. Chattopadhyay, and C.V. Shank, *Nucl. Instr. Meth. A* **341**, 351 (1994).
- [4] S. Chattopadhyay; and other articles in the same proceedings, *AIP Conf. Proc.* **356**, 15 (1996).
- [5] P. Kung et al., *Phys. Rev. Lett.* **73**, 967 (1994); M. Uesaka et al., *Phys. Rev. E.* **50**, 3068 (1994).
- [6] R.W. Schoenlein et al., submitted to *Science*, 1996
- [7] G. Fiocco and E. Thompson, *Phys. Rev. Lett.* **10**, 89 (1963); R. H. Milburn, *Phys. Rev. Lett.* **10**, 75 (1963).
- [8] T. Shintake, *Nucl. Inst. Meth.* **A311**, 453 (1992).
- [9] W.P. Leemans et al., *AIP Conf. Proc.* **335**, 209 (1995).
- [10] L. Wartski et al., *J. Appl. Phys.* **46**, 3644 (1975); D.W. Rule, *Nucl. Instr. Meth.*, **B24/25**, 901 (1987).
- [11] C. LeBlanc et al., *Opt. Lett.* **18**, 140 (1993).
- [12] Kodak Lanex fast $Gd_2OS_2:Tb$.
- [13] D.P. Trauernecht and R. Van Metter, *SPIE Proc.* **914**, 100 (1988).
- [14] Photometrics CH250 camera with a 512x512 Thomson 7895B chip and operated in a slow scan, pixel binned mode.
- [15] J. Bengtson, W. Leemans, and T. Byrne, *Proc. 1993 Particle Accelerator Conf.*, 567(1993).
- [16] H. Groter and F. Iselin, "The MAD program", CERN/SL/90-13 (1993).

Figure Captions

Figure 1. Schematic of the experimental set-up.

Figure 2. ▲ - vertical line-out through an OTR image of the electron beam; ■ - x-ray yield vs. vertical laser beam position.

Figure 3. a) False color CCD image of the spatial profile of a 30 keV x-ray pulse on the phosphor screen; b) ■ - horizontal lineout and fitting curve (solid line), ▲-vertical lineout and fitting curve (dashed line)

Figure 4. a) x-ray yield vs. delay time between laser and electron beam; b) time resolved OTR image from a streak camera.

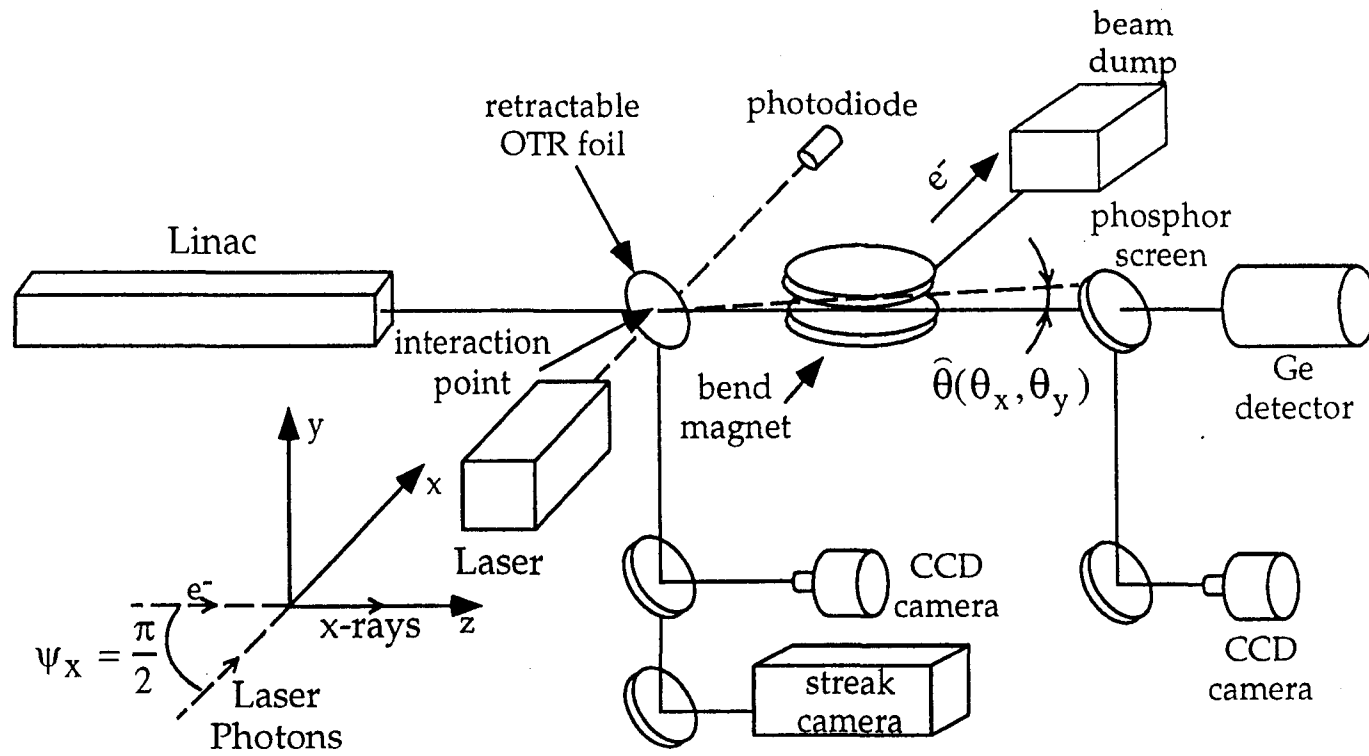
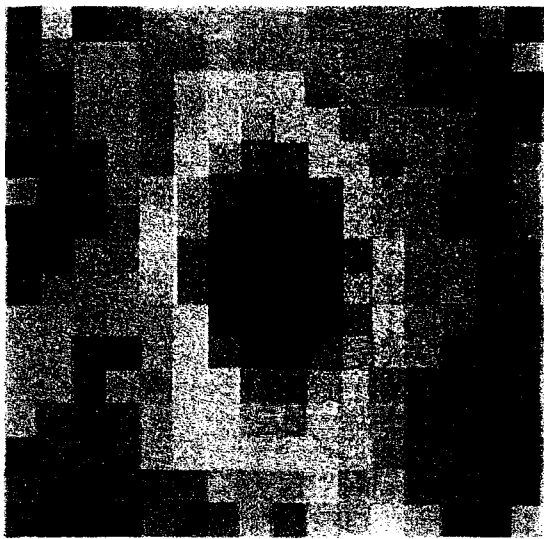
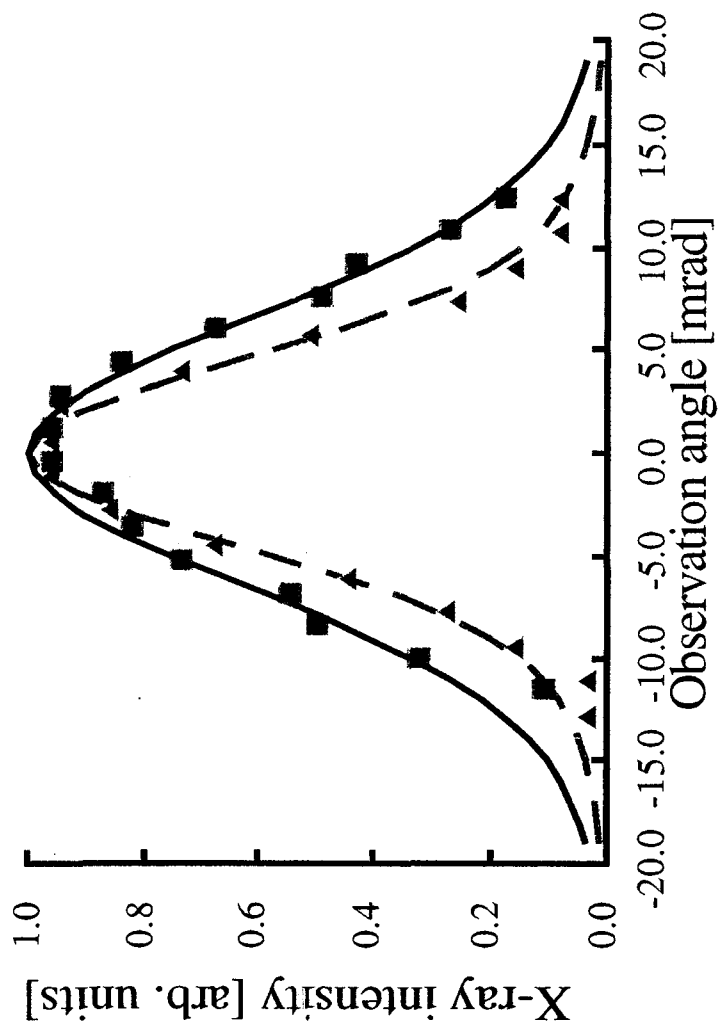


Figure 1



(a)



(b)

Figure 2

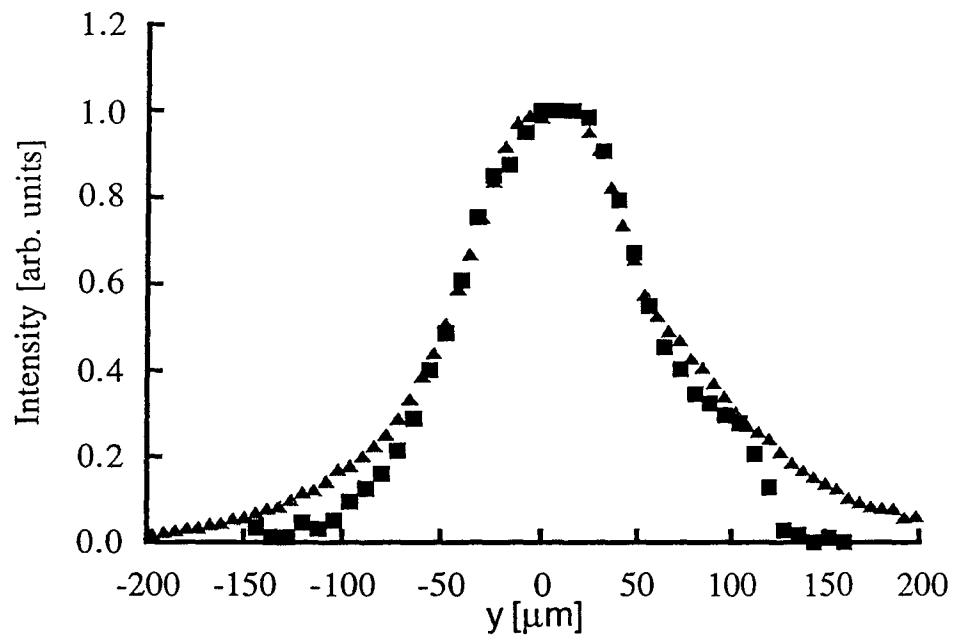


Figure 3

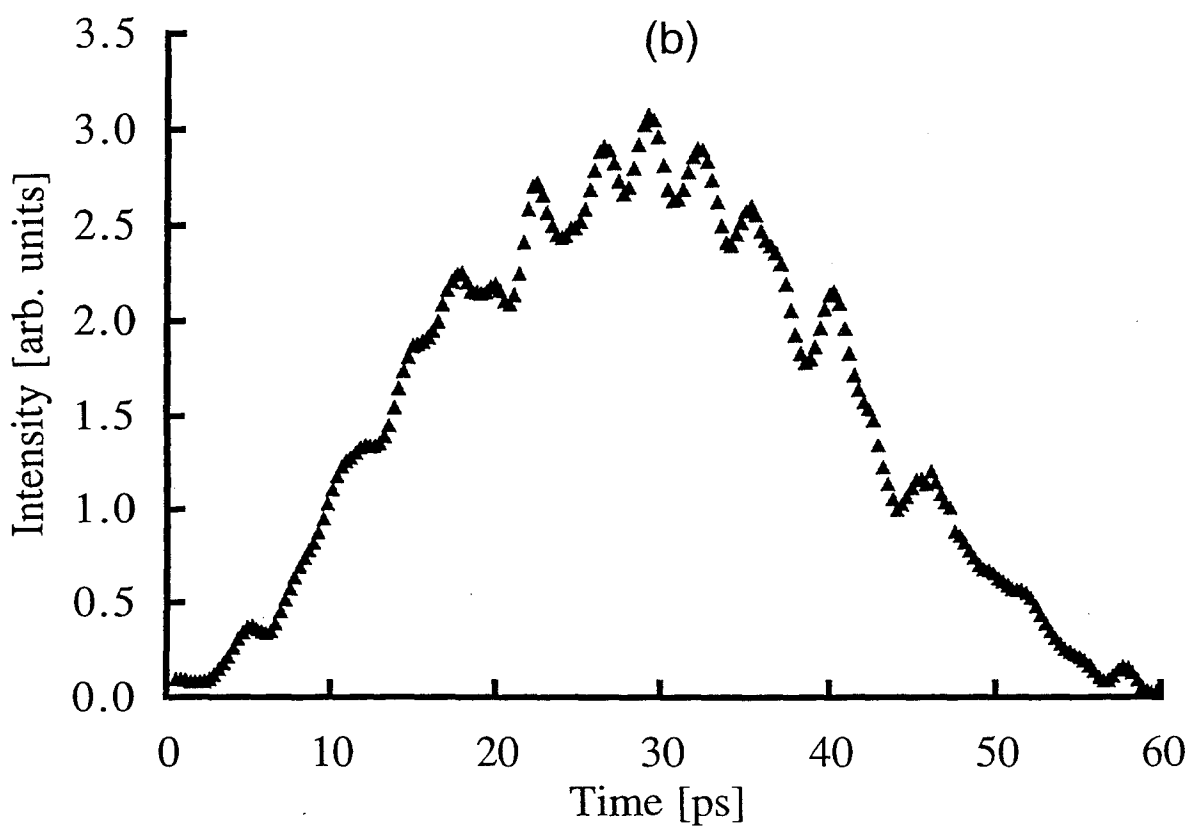
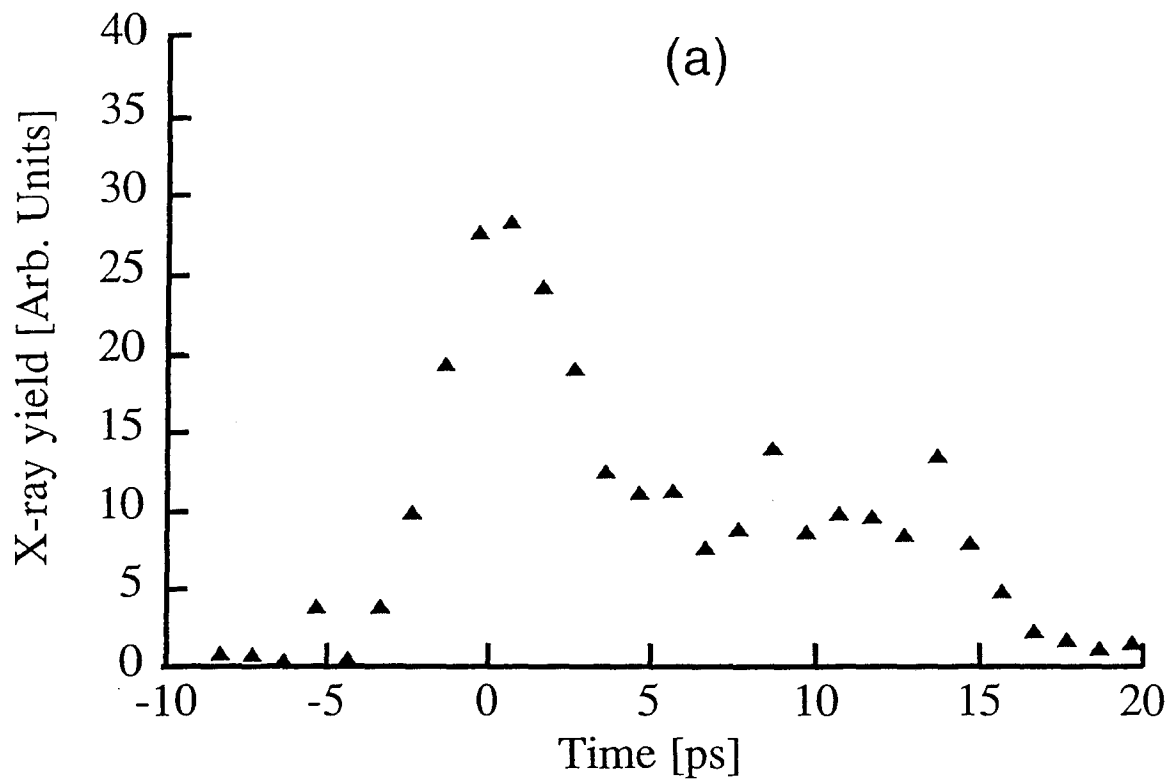


Figure 4